Cerebral Cortex, June 2017;27: 3346–3359

doi: 10.1093/cercor/bhx070
Advance Access Publication Date: 23 March 2017
Original Article

ORIGINAL ARTICLE

Occipital White Matter Tracts in Human and Macaque

Hiromasa Takemura[1,2], Franco Pestilli[3], Kevin S. Weiner[4], Georgios A. Keliris[5,6], Sofia M. Landi[7], Julia Sliwa[7], Frank Q. Ye[8], Michael A. Barnett[4], David A. Leopold[8], Winrich A. Freiwald[7], Nikos K. Logothetis[5] and Brian A. Wandell[4]

[1]Center for Information and Neural Networks (CiNet), National Institute of Information and Communications Technology, and Osaka University, Suita-shi, Osaka 565-0871, Japan, [2]Graduate School of Frontier Biosciences, Osaka University, Suita-shi, Osaka 565-0871, Japan, [3]Department of Psychological and Brain Sciences, Indiana University, Bloomington, IN 47405, USA, [4]Department of Psychology, Stanford University, Stanford, CA 94305, USA, [5]Max Planck Institute for Biological Cybernetics, 72072 Tübingen, Germany, [6]Bio-Imaging Laboratory, Department of Biomedical Sciences, University of Antwerp, Wilrijk 2610, Belgium, [7]Laboratory of Neural Systems, The Rockefeller University, New York, NY 10065, USA and [8]Neurophysiology Imaging Facility, National Institute of Mental Health, National Institute of Neurological Disorders and Stroke, National Eye Institute, National Institutes of Health, Bethesda, MD 20814, USA

Address correspondence to Hiromasa Takemura, Center for Information and Neural Networks (CiNet), National Institute of Information and Communications Technology, and Osaka University, Suita-shi, Osaka 565-0871, Japan. Email: htakemur@nict.go.jp

Abstract

We compare several major white-matter tracts in human and macaque occipital lobe using diffusion magnetic resonance imaging. The comparison suggests similarities but also significant differences in the tracts. There are several apparently homologous tracts in the 2 species, including the vertical occipital fasciculus (VOF), optic radiation, forceps major, and inferior longitudinal fasciculus (ILF). There is one large human tract, the inferior fronto-occipital fasciculus, with no corresponding fasciculus in macaque. We could identify the macaque VOF (mVOF), which has been little studied. Its position is consistent with classical invasive anatomical studies by Wernicke. VOF homology is supported by similarity of the endpoints in V3A and ventral V4 across species. The mVOF fibers intertwine with the dorsal segment of the ILF, but the human VOF appears to be lateral to the ILF. These similarities and differences between the occipital lobe tracts will be useful in establishing which circuitry in the macaque can serve as an accurate model for human visual cortex.

Key words: comparative study, diffusion MRI, vertical occipital fasciculus, visual cortex, white matter

Introduction

The macaque monkey has been an important model for understanding human vision. The 2 species perform at similar levels on many basic sensory tasks, such as color, motion, and spatial discriminations (De Valois and Jacobs 1968; De Valois et al. 1974; Newsome et al. 1989; Miura et al. 2006; Horwitz 2015), or categorization of objects (Sigala et al. 2002; Rajalingham et al. 2015). Some performance differences between human and macaque vision have also been described (Gellman et al. 1990; Zarco et al. 2009; Lindbloom-Brown et al. 2014; Horwitz 2015). A substantial literature compares human and macaque functional cortical responses to visual stimuli (Brewer et al. 2002; Tsao et al. 2003, 2008; Orban et al. 2004; Sasaki et al. 2006; Kriegeskorte et al. 2008; Wade et al. 2008; Pinsk et al. 2009; Mantini et al. 2012;

Okazawa et al. 2012; Polosecki et al. 2013; Goda et al. 2014; Kolster et al. 2014; Russ and Leopold 2015; Lafer-Sousa et al. 2016). There are similarities and differences in the functional responses, as well (Tootell et al. 2003; Wandell and Winawer 2011; Vanduffel et al. 2014).

The anatomical connections to visual cortex are important data for understanding the similarities and differences of the functional organization in the 2 species. It is well established that the physiological properties of individual neurons are similar throughout cortex, with large variations in neuronal responses arising substantially from differences in their connections. For instance, Wernicke's and Geschwind's classic theory of Connectionism emphasizes the important role of the white-matter axon bundles (fascicles, tracts) in defining the long-range neuronal connections (Catani and Ffytche 2005; Catani and Thiebaut de Schotten 2012). These tracts establish critical features of the brain's information processing (Bullock et al. 2005; Fields 2008a, 2008b, 2015; Wandell and Yeatman 2013). Comparing the anatomical connections in the 2 species may help us specify which macaque behaviors and responses are a good model for human and which are not.

Diffusion magnetic resonance imaging (dMRI) and tractography algorithms provide an excellent opportunity to better understand the organization of major white-matter tracts (Catani et al. 2002; Mori and Zhang 2006; Schmahmann et al. 2007; Catani and Thiebaut de Schotten 2012; Craddock et al. 2013; Wandell and Yeatman 2013; Wandell 2016). These methods assess the large-scale organization of the major white-matter tracts, including their relative positions of the tracts, their relative sizes, and the positions of the estimated tract endpoints with respect to the visual field maps (Greenberg et al. 2012; Takemura et al. 2016b; Rokem et al. 2017). The goal of this study is to shed light on how the pattern of long-range white-matter tracts contributes to the functional and behavioral similarities and differences between human and macaque visual system. This work is part of a growing literature using dMRI and tractography to compare the white-matter tracts between the 2 species (Schmahmann et al. 2007; Rilling et al. 2008; Thiebaut de Schotten et al. 2011; Jbabdi et al. 2013; Li et al. 2013; Mars et al. 2016; van den Heuvel et al. 2016).

We report 3 principal findings. First, several white-matter tracts are homologous in the human and macaque occipital lobe. These are the optic radiation (OR), forceps major, and inferior longitudinal fasciculus (ILF). In contrast, we do not find support for the existence of a macaque tract homologous to the human inferior fronto-occipital fasciculus (IFOF), a relatively large tract in human.

Second, we describe the vertical occipital fasciculus (VOF), a major white-matter tract communicating between the dorsal and ventral streams (Takemura et al. 2016b). We focus on the VOF because other major tracts have been extensively described (Schmahmann et al. 2007), but until recently the VOF has been relatively neglected in both the human and macaque literature (Yeatman et al. 2013, 2014; Duan et al. 2015; Wu et al. 2016; Weiner et al. 2016a; Takemura et al. 2016b; Kay and Yeatman 2017; Lee Masson et al. 2017). The diffusion measurements reveal a tract located in a position consistent with classical reports by Wernicke in an unnamed monkey species (Wernicke 1881). The dorsal and ventral endpoints of the VOF are near similar visual field maps in human and macaque. The VOF endpoint positions may be particularly important for understanding how information is communicated between the dorsal and ventral streams within the occipital lobe.

Third, we describe a difference in the relative position of several, large tracts in the occipital lobe: the VOF, ILF, and OR. In both human and macaque, the VOF is clearly located lateral to the OR. However, the macaque VOF (mVOF) crosses with the dorsal segment of the ILF, while the human VOF is more clearly distinct from human ILF in terms of tract position and endpoints.

Materials and Methods

MR Data Acquisition

The analyses are based on a diverse set of macaque and human measurements, pooled across several laboratories, and public data sets. The data sets have different spatial and angular resolution and image quality (see Supplementary Fig. 1). We analyze 4 different macaque data sets (M1–M4). Several of the key analyses rely on the macaque data with the highest resolution (M1, 250 μm isotropic).

We also analyze 10 human subjects, from 2 different data sets. One set of diffusion data was measured by the Human Connectome Project (HCP90, 5 subjects; Van Essen et al. 2013). To help identify the position of tract endpoints with respect to the fMRI-based visual field maps, we also used data from 5 subjects that had both diffusion and fMRI measurements from an additional data set (STN96). The experimental procedures for the experimental STN96 data obtained at Stanford were approved by the Stanford University Institutional Review Board. The MR data acquisition parameters and preprocessing pipeline are described in Supplementary Information (see "Supplementary Materials and Methods").

Tractography and Fascicle Evaluation

We used ensemble tractography (ET) to estimate the streamlines in the human and macaque data (Takemura et al. 2016a; https://github.com/brain-life/ensemble_tractography). This method begins by generating a large set of candidate streamlines using MRtrix (Tournier et al. 2012). The candidate connectome is created using the entire white-matter volume as a seed region. We generated candidate streamlines using probabilistic tractography and 5 curvature thresholds (minimum radius of curvature, 0.25, 0.5, 1, 2, and 4 mm; Takemura et al. 2016a). We set other parameters as default (step size: 0.2 mm; maximum length: 200 mm; minimum length: 10 mm). We generated a total of 10 000 000 streamlines for the large human brain and 2 500 000 streamlines for the smaller macaque brain. Finally, we used linear fascicle evaluation (LiFE; Pestilli et al. 2014; Caiafa and Pestilli 2015; 2017) to optimize the candidate connectome. This procedure removes the streamlines that make no significant contribution to explaining the diffusion measurements. Further technical detail about tractography and fascicle evaluation is described in Supplementary Information (see "Supplementary Materials and Methods").

Cortical Map Identification

Human Data

For the STN96 data set, we identified the location of cortical areas (visual field maps) using fMRI data and the population receptive field method (Dumoulin and Wandell 2008; Wandell and Winawer 2011). We identified the border between visual areas (V1, V2, V3, hV4, V3A/B, VO, LO, and IPS-0) based on the reversal of polar angle, eccentricity, and anatomical landmarks (Press et al. 2001; Dougherty et al. 2003; Brewer et al. 2005;

Larsson and Heeger 2006; Amano et al. 2009; Witthoft et al. 2014; Winawer and Witthoft 2015). The IPS-0 map could be only identified in one representative subject (H6). Technical details of the method are described in previous publications (Dumoulin and Wandell 2008; Amano et al. 2009; Winawer et al. 2010; Takemura et al. 2012, 2016b).

For the HCP90 data set, we identified the location of visual field maps based on the surface-based probabilistic atlas proposed by Wang et al. (2015). We adapted the visual field maps defined in the atlas (V1/V2/V3, V3A/B, hV4, LO, and IPS-0) for the T_1-weighted image in individual HCP90 data set based on surface-based registration.

Macaque Data

We used the Saleem and Logothetis D99 digital macaque brain atlas (Saleem and Logothetis 2012; Reveley et al. 2016) to identify areas in macaque visual cortex (V1, V2, V3, V3A, V4d, V4v, MT, and TEO). This atlas was originally defined by comparison between the histology and anatomical MRI data (Saleem and Logothetis 2012). We then transformed this MRI-based atlas into individual macaque brain data by using nonlinear alignment (Reveley et al. 2016; https://afni.nimh.nih.gov/pub/dist/atlases/macaque/macaqueatlas_1.2a/). Further technical details and the performance of the atlas fitting method are discussed in a previous publication (Reveley et al. 2016).

Tract Identification

For both human and macaque data, we identified major white-matter tracts in occipital cortex using waypoint Region of Interests (ROIs) drawn on the structural MRI images based on of anatomical prescriptions (Catani et al. 2002; Wakana et al. 2004). The streamlines that pass through a pair of ROIs are considered as potential members of a given tract. We describe the position of macaque waypoint ROIs in Supplementary Figure 2, as well as stereotactic coordinates of ROI position in AC coordinate on the D99 digital macaque brain atlas (Reveley et al. 2016).

The set of potential streamlines is refined by removing outliers. These are streamlines that meet the following criteria: 1) the streamline length ≥3 SD longer than the mean streamline length in the tract, 2) the streamline position is ≥3 SD away from the mean position of the tract (Yeatman et al. 2012b). We relaxed these criteria for the IFOF (4 SD for both length and position), because human IFOF streamlines are relatively sparse and distributed.

There were a few additional processing steps. First, we used ConTrack (Sherbondy et al. 2008a) to identify the human OR. There are known challenges to estimate human OR using a standard whole-brain tractography, particularly on the tracking of crossing fiber regions around Meyer's loop (Chamberland et al. 2017). We chose ConTrack as a dedicated method for identifying human OR because ConTrack successfully reconstructs the human OR, including Meyer's loop, in a consistent manner with postmortem anatomy (Sherbondy et al. 2008a, 2008b).

Second, in both human and macaque VOF, we added the constraint that streamlines must be dorsal–ventral between the 2 ROI waypoints. Streamlines whose path deviated more than 2 SD from the mean direction of the VOF streamlines (Takemura et al. 2016b) were deleted. Finally, tract visualization used the Matlab Brain Anatomy toolbox (https://github.com/francopestilli/mba; Pestilli et al. 2014). Further technical details on tract identification method are described in Supplementary Information (see "Tract identification method" in Supplementary Information on Materials and Methods).

Virtual lesions

We used the virtual lesion method (Pestilli et al. 2014; Leong et al. 2016; Takemura et al. 2016b) to evaluate the evidence supporting the existence of the mVOF. Specifically, we compared the change in prediction accuracy (root mean squared error; RMSE) for diffusion signal between the optimized connectome and a lesioned connectome with the streamlines of interest removed. The RMSE is compared in all voxels touched by the lesioned streamlines, the mVOF in this case. The complete set of streamlines that contribute to the prediction of the diffusion measurements in these voxels is called the path-neighborhood of the mVOF. The path-neighborhood includes the mVOF itself and the other streamlines that pass through the mVOF voxels. We measure the distribution of RMSE values in the mVOF voxels when using the entire path-neighborhood, and then we remove the mVOF and solve for the weights with the remaining streamlines. The supporting evidence is the difference in the mean RMSEs divided by the joint standard deviation, which we call the strength of evidence, *S* (see Pestilli et al. 2014). Technical details of the method are described elsewhere and through our open-source software (https://github.com/francopestilli/life; Pestilli et al. 2014; Takemura et al. 2016b). We note that the computational implementation of LiFE used in this study (Caiafa and Pestilli 2015; 2017) is not identical to the implementation in the original paper (Pestilli et al. 2014; Takemura et al. 2016b). While the numerical values of the virtual lesion are not precisely the same to those in earlier publications, the values and conclusions are consistent.

Relating the VOF endpoint and cortical maps

Streamlines terminate at the boundary between white and gray matter. We measured the distance between tract endpoints and gray matter voxels to identify the cortical areas closest to the tract endpoints. Specifically, we collected the coordinates of the endpoints of the VOF streamlines and computed the distance between the coordinates of the endpoint and gray matter voxels. Then, for each gray matter voxel, we counted the number of endpoints within a threshold distance (human data: 3 mm, macaque data: 2 mm). We plot the normalized endpoint counts on the smoothed cortical surface (Fig. 5).

This analysis has some limitations, derived from the challenges in associating the cortical surface and tract endpoints (Reveley et al. 2015). This analysis measures only the general proximity between cortical maps and tract endpoints. It is not a definitive estimate of the fiber projections into cortical gray matter regions.

Results

We begin by comparing the spatial arrangement of the major white-matter tracts in both human and macaque visual cortex. We focus much of our attention on a tract that has been little studied: the human and macaque VOF (see Yeatman et al. 2014). Specifically, we identify its position with respect to other tracts and the location of its endpoints with respect to the cortical maps.

Comparison of Major Occipital Tract Positions

Figure 1 compares the general organization of the major occipital tracts in macaque (Fig. 1*A*) and human (Fig. 1*B*). We consistently identified the major tracts (OR, ILF, forceps major, and VOF) from both data sets (see Supplementary Fig. 3 for the examples in other macaque and human data sets). With the exception of the mVOF, these tracts are reported in previous studies in human (Wakana et al. 2004; Catani and Thiebaut de Schotten 2008, 2012;

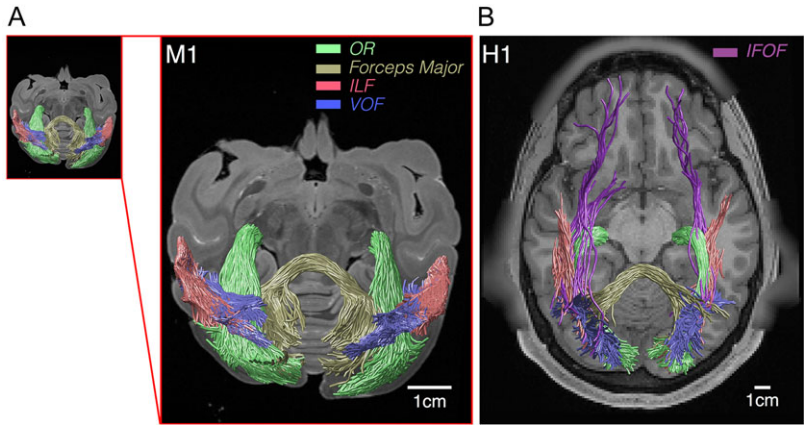

Figure 1. Major white-matter tracts with at least one endpoint in occipital cortex. Axial view of major white-matter tracts (ILF, red; IFOF, purple; OR, green; Forceps Major, dark yellow; VOF, blue) overlaid on anatomical image in a representative macaque (*A*, subject M1, ex vivo) and human (*B*, subject H1, HCP90 data set). The small panel in the left side in panel A indicates the size of the macaque tracts in an identical spatial scaling with human figure.

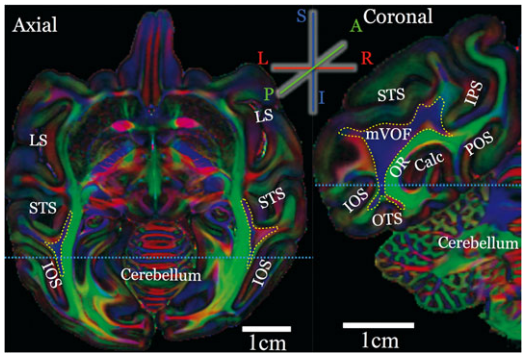

Figure 2. The position of the mVOF. The position of the mVOF identified in PDD map (subject M1, ex vivo). The color scheme depicts the PDD in each voxel (blue, superior–inferior; green, anterior–posterior; red, left–right). In the axial slice (left panel), we could see the white-matter portion with predominantly superior–inferior diffusion signal between superior temporal sulcus (STS) and inferior occipital sulcus (IOS). In the coronal slice (right panel), this region is located lateral to the calcarine sulcus and the OR (which has anterior–posterior PDD, green). Scale bar (white) in each panel indicates 10 mm. Light blue dotted line in left panel indicates the position of coronal slice in the right panel, vice versa. LS, lateral sulcus; IPS, intraparietal sulcus; Calc, calcarine sulcus; POS, parieto-occipital sulcus; OTS, occipito-temporal sulcus.

Martino and Garcia-Porrero 2013; Yeatman et al. 2013; Takemura et al. 2016b) and macaque (Schmahmann and Pandya 2006; Schmahmann et al. 2007). We discuss the VOF in more detail in the next section.

There is a significant difference between the major occipital tracts in human and macaque: we do not find evidence for an IFOF in macaque dMRI data with highest resolution (subject M1, 250 μm isotropic voxels; see Supplementary Fig. 2 for IFOF waypoint ROI definition). This is consistent with previous studies showing evidence for the existence of the IFOF in humans (Curran 1909; Catani and Thiebaut de Schotten 2008; Martino et al. 2010a, 2010b, 2011; Sarubbo et al. 2013; Forkel et al. 2014; Pestilli et al. 2014), but no evidence for this tract in macaques (Schmahmann and Pandya 2006; Schmahmann et al. 2007; but see Mars et al. 2016).

Identification of mVOF

Figure 2 shows the principal diffusion direction (PDD) map in the highest resolution ex vivo macaque dMRI data set (subject M1, 250 μm isotropic voxels; see Supplementary Fig. 2 for other slices). The PDD map has been used to identify the position of the VOF in human studies (Pajevic and Pierpaoli 1999; Wakana et al. 2004; Yeatman et al. 2013; Takemura et al. 2016b). Inspection of the PDD images clearly reveals the position of several major tracts; such as the OR and forceps major (Fig. 2 and Supplementary Fig. 4).

The PDD maps in this high-resolution data set clearly identify the major macaque pathways including a pathway seemingly homologous to the human VOF. Specifically, the data in Figure 2 reveal tracts with a superior–inferior diffusion direction (blue) in the lateral occipital white matter (outlined). The blue PDD indicates the presence of a vertical tract communicating between dorsal and ventral visual cortex. The ventral portion of this tract is located between IOS and the STS (left panel, axial view, Fig. 2). This tract is lateral to the calcarine sulcus and the OR (green regions in right panel, Fig. 2). This tract is also identifiable from PDD map in other slices (Supplementary Fig. 4). Hereafter, we call this tract macaque vertical occipital fasciculus (mVOF). We consistently identified the core portion of this tract from the PDD map in the data set from living and postmortem macaque brain with coarser spatial resolution (see Supplementary Fig. 12 and "Instrumentation and Acquisition Parameter Dependencies"). We also note that the mVOF position is qualitatively consistent with classical reports by Wernicke and others (Wernicke 1881; Bailey et al. 1944; Petr et al. 1949; see "Diffusion MRI Estimates of the mVOF are Consistent with Anatomical Studies" in Discussion).

Figure 3A shows the estimated mVOF (see Materials and Methods). It is located on the anterior-lateral side of the lunate sulcus dorsally, and its ventral endpoints are near the occipito-temporal sulcus (OTS). We observed the core of the mVOF in this position for all 8 hemispheres from the macaque brains (see Supplementary Fig. 12 for more examples). Figure 3B is the human VOF identified from HCP90 data set, shown for a comparison. Note the very different scales. The topological position and dorsoventral endpoints of the VOF are similar in the 2 species, as elaborated below (see "Cortical Regions Near the mVOF Endpoints").

Statistical Evidence in Support of the mVOF Tract

We evaluate the strength of evidence supporting the existence of the mVOF using the virtual lesion method (Pestilli et al. 2014;

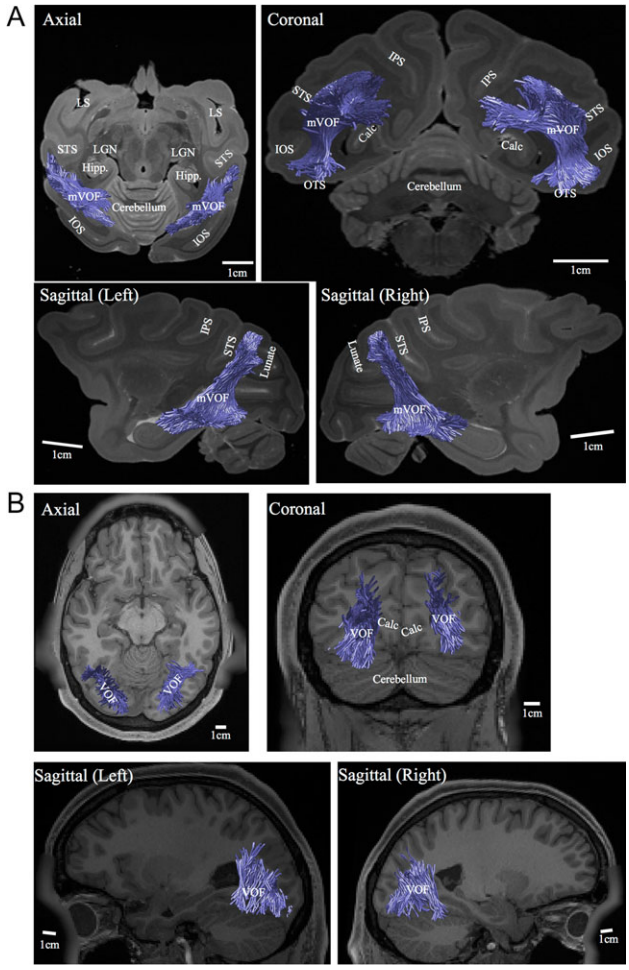

Figure 3. Human and macaque VOF identified using tractography. (*A*) mVOF identified using tractography, overlaid on nondiffusion weighted ($b = 0$) image (subject M1; left top, axial slice; right top, coronal slice; bottom, sagittal slices). Lunate, lunate sulcus; Hipp, hippocampus. Other conventions are identical to those in Figure 2. (*B*) Human VOF identified using tractography, overlaid on T_1-weighted image (subject H1, HCP90 data set). Scale bar (white line) in each panel indicate 10 mm.

Leong et al. 2016; Takemura et al. 2016b) that compares how well 2 connectome models predict the diffusion signal in the voxels of a tract of interest, mVOF. The unlesioned model contains all streamlines in the voxels of the mVOF. The lesioned model has the streamlines of the tract of interest removed. We compare the RMSE of the 2 models in the mVOF voxels. We quantify the strength of evidence (S) in support of the tract by calculating the RMSE divided by the standard deviation of the RMSE (calculated by bootstrapping; Pestilli et al. 2014).

We measured clear differences in the RMSE of unlesioned and lesioned models in the very high-quality macaque data set (M1). The strength of evidence for the mVOF pathway in the right hemisphere of M1 is S = 14.09 (Fig. 4A). The value is larger, S = 25.64, in the left mVOF. The scatter plot in Figure 4B compares the RMSE of the 2 models for each voxel; the plot suggests that the evidence, S, arises from a subset of the mVOF voxels that have a substantially larger RMSE in the lesioned model. Thus, in addition to visible evidence on PDD maps (Fig. 2 and Supplementary Fig. 4), the virtual lesion analysis quantitatively supports the hypothesis that the mVOF exists in subject M1.

Cortical Regions Near the mVOF Endpoints

Despite some differences in visual field map organization between humans and macaques, the position and course of the VOF appear consistent between the 2 species; the VOF endpoints are near V3A in the dorsal stream, and V4 in the ventral stream. These similarities in cortical endpoints suggest that the mVOF is homologous to human VOF.

We identified the cortical maps near the endpoints of the VOF in humans and macaques. In humans, visual field maps were identified using fMRI as reported in a previous study (Takemura et al. 2016b) as well as using a surface-based atlas (Wang et al. 2015). In macaques, visual areas were identified using a standard MRI-based atlas (Saleem and Logothetis 2012). The atlas-based method is rather precise for the simple macaque brain (Reveley et al. 2016). For the human brain, the atlas-based method was further confirmed by visual field map measurements in the living human brains (see below). Tract cortical endpoints were computed by counting the number of VOF streamlines exhibiting endpoints near each gray matter voxel (tract endpoint density, see Materials and Methods; Takemura et al. 2016b). Normalized streamline endpoint density

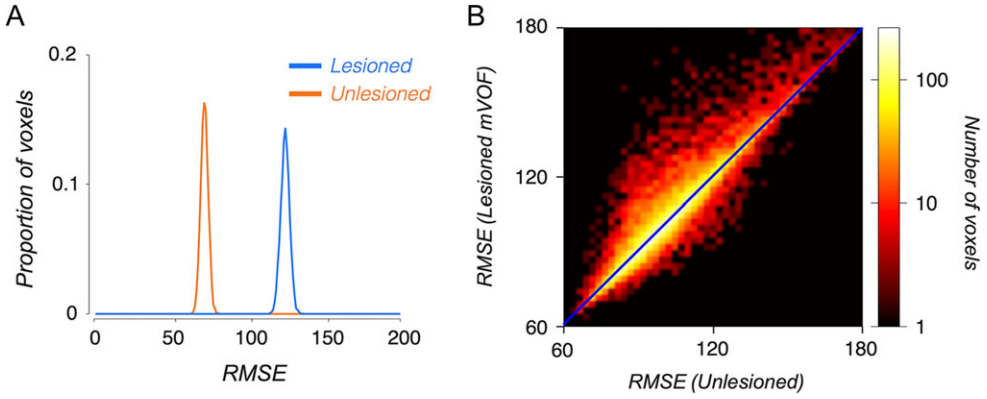

Figure 4. Statistical evidence supporting the existence of the mVOF. (*A*) The bootstrapped RMSE distributions for the unlesioned (orange) and lesioned (blue) models. The RMSE is calculated for voxels in the right mVOF in subject M1 (see Material and Methods). The 2 distributions are widely separated (S = 14.03). (*B*) Two-dimensional histogram comparing the RMSE between unlesioned (abscissa) and lesioned (ordinate) models (right mVOF voxels in M1). Color map indicates the number of voxels. The increased error in the lesioned model arises from a subset of the voxels that have larger RMSE for the lesioned compared with the full model (upper left).

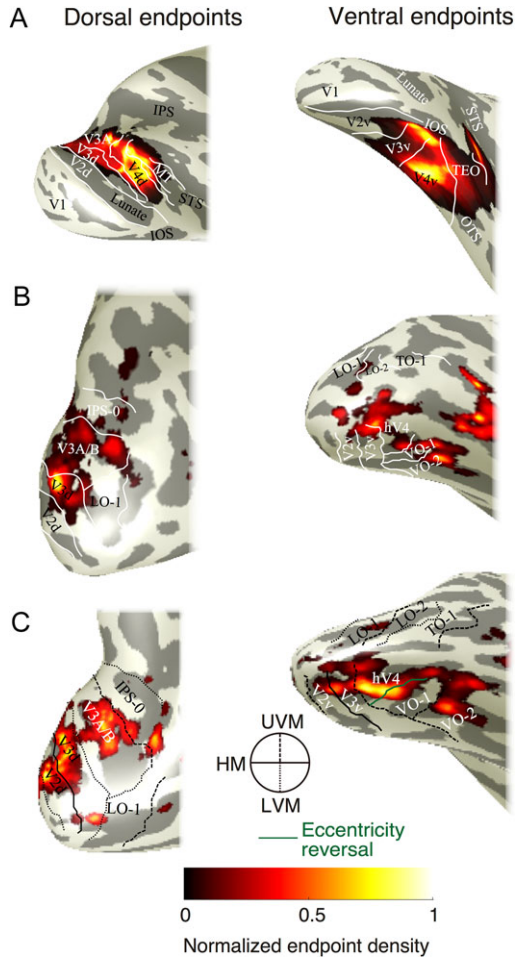

Figure 5. Cortical visual maps near VOF endpoints in human and macaque. (*A*) Cortical maps near the mVOF endpoint (subject M1, right hemisphere). In this plot, we calculated the spatial distance between mVOF endpoints and gray matter voxels, and counted the number of mVOF streamlines having endpoints close to the gray matter voxel (see Materials and Methods). The boundaries between visual areas are manually identified using an MRI-based atlas (Saleem and Logothetis 2012). We observed the putative mVOF termination near V3A and V4d dorsally, as well as V4v and TEO ventrally. See Supplementary Fig. 5 for more examples. (*B*) Cortical maps near human VOF endpoint in a representative hemisphere from HCP90 data set (subject H1, right hemisphere). The boundaries between cortical areas are estimated using a surface-based probabilistic atlas (Wang et al. 2015). (*C*) Cortical maps near human VOF endpoints in relation to visual field maps estimated individually using fMRI (Dumoulin and Wandell 2008; STN96 data set, subject H4, right hemisphere). The boundaries between cortical areas are defined by the boundaries of polar angle and eccentricity estimated by fMRI-based visual field mapping (see captions at the center; circular inset; UVM, upper vertical meridian; HM, horizontal meridian; LVM, lower vertical meridian).

was superimposed on the cortical surface (Fig. 5; see Materials and Methods).

Figure 5*A* shows the mVOF terminations in several visual field maps (right hemisphere, subject M1). The mVOF terminates near the anterior portion of the lunate sulcus dorsally and the OTS ventrally. The left panel of Figure 5*A* shows maps near dorsal mVOF endpoints. The region includes V3A, V4d/DP, and possibly MT (see Supplementary Fig. 5 for the results in left hemisphere). The right panel of Figure 5*A* shows the maps near ventral mVOF endpoints. The endpoints are near the OTS, which is mostly V4v. There are some endpoints near the anterior portion of the OTS, which may correspond to TEO (Saleem and Logothetis 2012; Kolster et al. 2014; see Supplementary Fig. 5 for the results in left hemisphere). In the supplementary analyses, we show that the estimates of cortical endpoint positions do not change substantially as we vary the waypoint ROI positions (Supplementary Fig. 6). The estimates of cortical endpoint positions, however, do depend on the spatial resolution of the diffusion MRI data (see "Instrumentation and Acquisition Parameter Dependencies"; Supplementary Fig. 13).

Figure 5*B* and *C* describe the results on the right hemisphere in 2 representative human data sets (subject H1, HCP90 data set; subject H4, STN96 data set). One of the data sets (STN96) was used previously (Takemura et al. 2016b), but the present analysis differs because we now use ET methods (Takemura et al. 2016a; see Materials and Methods). The new analysis confirms the previous results (Takemura et al. 2016b), showing that the dorsal human VOF endpoints are near V3A and V3B, V3d and IPS-0, whereas the ventral endpoints are near human V4, VO-1, and neighboring maps. This pattern is consistent across data sets (HCP90, Fig. 5*B* and STN96, Fig. 5*C*; see Supplementary Figs 7 and 8 for more examples). Human VOF endpoints supported by the HCP90 data set generally cover larger portions of cortical maps presumably because of the smaller voxel size.

VOF Position with Respect to Other Tracts

Figure 6*A* shows the position of the VOF with respect to the OR and the ILF. In human and macaque, the VOF is located lateral to the OR and the 2 tracts are clearly distinguishable (Fig. 6*A*, top panels). This has also been reported in classical studies of postmortem human and macaque (Wernicke 1881; Déjerine 1895).

In human, the ILF and VOF streamlines can be well separated and identified; the VOF streamlines are lateral to the ILF streamlines (Fig. 6*A*, bottom image; see Supplementary Fig. 9 in other example from STN96 data set). Relatively few ILF streamlines cross with VOF streamlines, and the crossings occur at slightly different positions depending on the position of the waypoint ROIs (Supplementary Fig. 10).

In macaque, the ILF and VOF streamlines pass through many of the same voxels (Fig. 6*A*). The mVOF streamlines are distinguished from the ILF mainly by the position of their endpoints on the cortical surface (Fig. 6*B*). In macaque, the mVOF streamlines connect positions on dorsal and ventral posterior cortex. These are distinguished from ILF streamlines which have one endpoint in posterior cortex and a second endpoint in anterior cortex. Unlike the human, in which the streamlines themselves can be segregated, the macaque streamlines of the VOF and ILF are mainly distinguished by their endpoints.

The pattern in macaque did make us consider whether the ILF and VOF might be a single functional tract, perhaps supporting the same cortical processing goals. But given 1) the 2 were segregated historically, 2) the different patterns of terminations, and 3) the clear separation in human, we prefer to distinguish the macaque VOF and ILF streamlines (see "The Spatial Organization of the VOF and ILF in Human and Macaque" in Discussion). We provide a summary plot of the endpoint overlap between VOF and ILF streamline endpoints in Supplementary Figure 11.

Instrumentation and Acquisition Parameter Dependencies

The ability to resolve different tracts, estimate their sizes, and locate their endpoints depends on the spatial and angular resolution of the acquisition (Kim et al. 2006; Roebroeck et al. 2008;

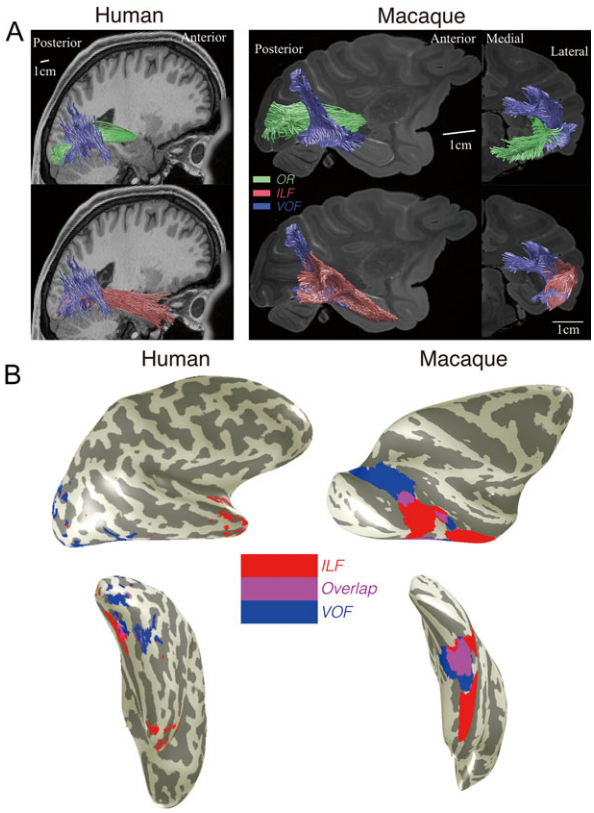

Figure 6. Human-macaque comparison of VOF position with respect to other tracts. (*A*) Spatial relationship between the OR (green), the ILF (magenta), and VOF (blue) in human and macaque. Macaque tracts are depicted from 2 different viewpoints (sagittal and coronal). (*B*) VOF and ILF cortical endpoints in human and macaque in the right hemisphere (human, subject H1 from HCP90 data set; macaque, subject M1), shown as cortical mesh representation from 2 different viewpoints. Color on the mesh indicates the approximate position of the ILF, VOF endpoints, and their overlap (red: ILF, blue: VOF, purple: overlap). See Supplementary Figure 11 for the summary statistics on the estimated overlap.

Berman et al. 2013; Sotiropoulos et al. 2013, 2016; Pestilli et al. 2014; see also Lebel et al. 2012). The quality of the postmortem data from M1 (Thomas et al. 2014; Reveley et al. 2015) is far beyond the other data sets. However, data collected from living brains offer additional opportunities even if it is limited in resolution (see "Combining Postmortem Anatomical Data with In Vivo Diffusion MRI" in Discussion). Here we tested what we can identify in relatively lower-resolution data sets from macaque brains.

Supplementary Figure 12A depicts the PDD map from macaque brain in other dMRI data sets. We can identify the mVOF (blue, superior–inferior) and the OR (Supplementary Fig. 12A; see Supplementary Fig. 14 for a comparison in other slice selections) from all data sets. The result suggests that the core portion of the mVOF can be consistently identified in all macaque data sets, including in vivo data. While the data sets are qualitatively consistent, the estimates of the spatial extent of mVOF differ across data sets, presumably because of the partial volume effect in lower-resolution data (Supplementary Fig. 12B).

The estimates of cortical endpoints also depend on spatial resolution. Supplementary Figure 13 compares the cortical maps near mVOF endpoints among the data sets. While the center of the mVOF endpoints is consistent, mVOF endpoints in subject M1 (higher-resolution data) span a larger spatial extent on the cortical surface. In lower-resolution data, we particularly miss cortical endpoints in the gyrus between IOS and OTS. The lower spatial resolution data is vulnerable to partial volume effects with gray matter and the superficial U-fiber system (Reveley et al. 2015; Vu et al. 2015).

Discussion

We used diffusion MRI data and tractography, in both human and macaque, to identify the major white-matter tracts with at least one occipital endpoint. In both species, we find apparently homologous tracts including the OR, forceps major, ILF, and VOF. We find no evidence for a macaque IFOF, consistent with previous reports (Schmahmann et al. 2007; Catani and Thiebaut de Schotten 2008).

We succeeded in identifying the mVOF, which has been little studied. The core portion of this tract is consistent across dMRI data sets obtained with different spatial resolutions and number of diffusion directions. The mVOF shares some similarities with human VOF, particularly with regard to the position of its endpoints with respect to the cortical maps. But the position of the VOF in relation to the ILF may differ between species.

Several Homologous Tracts, but No Evidence for a Homologous IFOF

There is a notable difference between human and macaque occipital white-matter tracts: the macaque dMRI data lack support for the IFOF (Schmahmann and Pandya 2006; Schmahmann et al. 2007), while the human dMRI supports the existence of an IFOF. The species difference concerning the IFOF has also been supported by classical and recent fiber dissection studies (Curran 1909; Martino et al. 2010a, 2010b, 2011; Sarubbo et al. 2013; Forkel et al. 2014). Furthermore, the statistical support for the human IFOF from dMRI data is very strong (Pestilli et al. 2014). We conclude that there is a significant interspecies difference with respect to the IFOF estimated by dMRI data, while there is a debate on the interpretation of the difference (Mars et al. 2016).

The functional significance of IFOF interspecies difference is an interesting question. One working hypothesis is that the IFOF is crucial for the rapid transmission of visual information to a semantic processing system in frontal cortex (Duffau et al. 2013). The much greater size of the human brain, which is 15 times the volume of macaque, allows for many new functions and the possibility that the IFOF provides visual information to many of these frontal circuits.

Diffusion MRI Estimates of the mVOF are Consistent with Anatomical Studies

Wernicke (1881) reported the existence of a tract ("senkrechte Occipitalbündel (fp)"; "vertical occipital bundle"; also termed as "perpendicular fasciculus") connecting dorsal and ventral occipital cortex. His schematic of an axial slice of the postmortem monkey brain is compared with the dMRI estimates of the PDD in macaque (Fig. 7, "fp" in the right panel). Wernicke (1881) described the position of "vertical occipital bundle" as lateral to the OR, which is consistent with PDD map (Fig. 2; see Supplementary Fig. 14 for additional examples from PDD maps in other macaque data set). In Wernicke's schematic diagram, the position of the vertical occipital bundle is surrounded by 2 sulci, which correspond to the modern definitions of the STS and the IOS. Thus, the existence and position of the mVOF derived from dMRI and tractography is consistent with Wernicke's classical postmortem study.

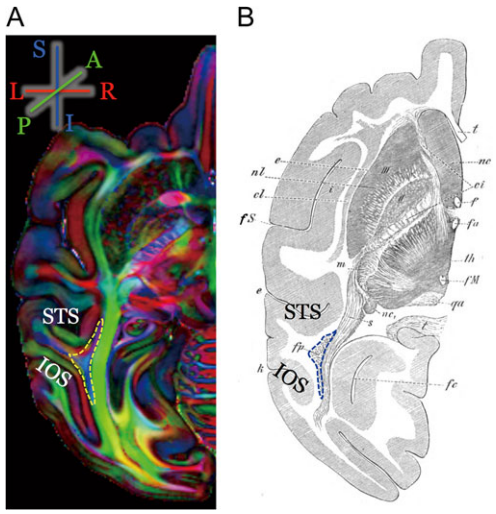

Figure 7. History of the mVOF. The comparison of the mVOF position in modern diffusion MRI data and Wernicke's study (Wernicke 1881). (*A*) The position of the mVOF in PDD map in the left hemisphere (subject M1). This slice is chosen to match the schematic diagram in Wernicke's study (right, *B*). While it is impossible to completely match the slice between modern data and classical work, the position of the mVOF (left) and "vertical occipital bundle" (fp, right panel) is qualitatively consistent; both are located between the STS ("e, Parallelfurche" in Wernicke) and IOS ("k, vordere Occipitalfurche" in Wernicke).

The dMRI derived mVOF is also consistent with tract degeneration studies conducted by Bailey et al. (1944). Specifically, they studied association pathways in *Macaca mulatta* by first injecting the neurotoxin in a target cortical site and then measuring the loss of electrophysiological signal following cortical damage. Using this method, Bailey and colleagues reported a pathway connecting the posterior end of the temporal cortex with both dorsal extrastriate cortex as well as the posterior portion of the inferior parietal lobule. Petr et al. (1949) further explored these tracts with comparable methods. They showed that this vertical pathway extends from dorsal visual cortex and nearby aspects of the inferior parietal lobe to macaque TEO, but not area TE. This observation is consistent with results from the present study showing that the mVOF has ventral endpoints within TEO, but not further anterior regions (Fig. 5). It is important to note that while the mVOF has not been widely examined in modern studies, these vertical connections were crucial for solidifying the division separating TEO from TE. These areas were not easily differentiated cytoarchitectonically in Von Bonin and Bailey's classic atlas (Petr et al. 1949; Iwai and Mishkin 1969).

Additionally, Bonin and colleagues (1942) suggested that the mVOF and ILF are compressed and intertwined within the occipital lobe of macaque. The VOF and ILF are clearly separable and orthogonal in human. Bonin and colleagues had very similar observations. In a summary of their strychnine measurements and Weigert stains in macaque, Bonin et al. write:

Wernicke's vertical bundle, running lateral of the ventricle, is well seen in the macaque wherein it was first recognized by Wernicke himself … there is much more room in the spacious white core of the occipital lobes of chimpanzee and man than in the sparse white matter of the macaque's occipital lobe. Hence the association fibers which are compressed into a compact bundle in the macaque, may be more diffusely spread out over a larger space in the higher primates… The experimental results suggest moreover that there are fibers passing from the dorsal part of the parastriate area to the temporal lobe. These may run first in the vertical occipital bundle of Wernicke, to sweep over into the inferior horizontal fasciculus in a ventral level. It should not be too difficult to test this assumption. (p. 179–183)

The evidence from the present study provides support for their hypothesis nearly 75 years later.

Evidence from recent studies provide further anatomical evidence for the mVOF. For example, in recent studies, Schmahmann and Pandya (2006) explored major white-matter tracts, including those in occipital cortex, in macaque brain using retrograde tracers. Schmahmann and Pandya directly relate the ILF to vertical fascicles when they write:

We have observed that fibers that are caudally situated in the vertical component of the ILF link the dorsal and ventral aspects of the occipital lobe and are equivalent to this vertical occipital system of Wernicke. (p. 450)

Their description of this fiber pathway is also consistent with what we observed in our dMRI data, showing the vertical occipital fiber connecting dorsal and ventral visual cortex which are less distinguishable from the ILF (Fig. 6).

There is a collection of tracer studies of the macaque that are consistent with this study. Ungerleider and Desimone (1986) reported a connection between MT and ventral V4. Distler et al. (1993) injected anterograde and retrograde tracers in macaque area TEO, and described bidirectional connections to dorsal areas, including V3d, V3A, V4d, and MT. Webster et al. (1994) explored the cortical connections in area TEO and TE, and reported that TEO is connected with V3A, whereas TE is predominantly connected to area LIPd, rather than V3A. More recently, Ungerleider et al. (2008) studied pathways terminating in macaque V4 using both anterograde and retrograde tracers. They described bidirectional connections between V3A, MT (dorsal), and ventral V4. These tracer studies suggest that the mVOF includes bidirectional information transmission between dorsal and ventral visual cortex. The streamline estimates here also show that the mVOF connects dorsal (V3A, V4d, and MT) and ventral areas (V4v, TEO).

Taken together, the mVOF streamlines follow a path that is consistent with macaque studies using fiber dissections, tract degeneration, Weigert stains, and tracers.

The VOF Cortical Endpoints and Visual Field Maps

The organization of the visual field map has been widely studied in both human and macaque, and scientists have proposed several principles describing the spatial distribution of function in visual cortex (Wandell et al. 2007). One prominent theory neuroscientists largely support is that relatively dorsal visual cortex processes spatial information relevant for action, whereas relatively ventral visual cortex processes categorical information relevant for object categorization and identification (Ungerleider and Mishkin 1982; Goodale and Milner 1992; Ungerleider and Haxby 1994). Various studies raise the likelihood of substantial interaction between dorsal and ventral visual cortex (Grill-Spector et al. 1998, 2000; Konen and Kastner 2008). The VOF provides an anatomical infrastructure supporting the interaction between dorsal and ventral visual cortex (Yeatman et al. 2014; Takemura et al. 2016b).

An additional functional role of the VOF arises from consideration of the representation of visual field information. In both human and macaque, V2 and V3 are separated into dorsal and

ventral components, and each represent a quarter of the visual field. However, midlevel visual maps contain hemifield representations, such as V3A/B, IPS-0, hV4, VO, LO in humans, and V3A in macaques. The macaque map organization anterior to V4v is controversial, but a recent study provides evidence for hemifield maps anterior to V4v and adjacent to TEO (Kolster et al. 2014). As endpoints of the VOF are near these hemifield maps, it is possible that the VOF has an essential functional role for transmitting upper and lower visual field information between dorsal and ventral visual field maps (Takemura et al. 2016b).

While the visual field maps in human and macaque are similar, they differ in several ways (Wandell and Winawer 2011; Kolster et al. 2014; Vanduffel et al. 2014). The differences include the relative size of V3 (Brewer et al. 2002; Dougherty et al. 2003; Lyon and Connolly 2012), the retinotopic organization of V4 (Brewer et al. 2005; Wade et al. 2008; Arcaro et al. 2009; Winawer et al. 2010; Goddard et al. 2011; Winawer and Witthoft 2015), and response selectivity in V3A (Tootell et al. 1997; Vanduffel et al. 2001). Also, the homology of some human maps, such as V3B (Smith et al. 1998; Press et al. 2001) and LO (Larsson and Heeger 2006; Amano et al. 2009; Silson et al. 2013), remains uncertain (but see Kolster et al. 2014). The difference in the spatial arrangement of maps between human and macaque may be related to the change in position and size of the VOF. The position of all these maps, and their size, makes it seem likely that the growth in the VOF and its change in position may have been coordinated with changes in the cortical organization.

The Spatial Organization of the VOF and ILF in Human and Macaque

Human and macaque VOF are similar in 2 critical ways. First, the endpoints of the VOF are near similar maps such as V3A in dorsal visual cortex and V4 in ventral visual cortex. Second, in both human and macaque, the VOF is located lateral to the OR and oriented in a direction perpendicular to the OR. These similarities suggest that the mVOF is a homologous pathway to the human VOF.

But there are also significant differences between these pathways that reflect some of the general differences between the macaque brain and the much larger human brain. First, the human VOF is greatly elongated in the anterior–posterior dimension compared with the mVOF, which is largely confined between the IOS and STS. The human VOF extends nearly to the posterior arcuate fasciculus (pAF; or vertical (posterior) segment of the arcuate; Catani et al. 2005; see Weiner et al. 2016b about the position of pAF with respect to VOF; see Fig. 8).

A second difference is that the macaque mVOF and ILF streamlines cross, but in human the estimated VOF streamlines are largely separate and lateral to the estimated ILF streamlines. This difference suggests a hypothesis regarding the evolution of the VOF that is related to the substantial cortical expansion in human (Fig. 8). The VOF may be the part of the ILF system in a common ancestor (right panel, Fig. 8). With the expansion of cerebral cortex and the increase in the number of midlevel visual areas, the VOF may have grown to the point where it became independent of the ILF system, shifting laterally and separating from the ILF. This hypothesis is speculative because it is difficult to exclude the possibility that the estimated human ILF streamlines separate from the VOF due to the limited ability to resolve crossing fibers in in vivo human data, limited ability of tractography algorithms, selection of acquisition and tractography parameters or waypoint ROI selection procedures. We include this speculation because it provides a hypothesis for future comparative studies, comparing high-resolution human and macaque anatomy data, that assess the evolution of the visual association areas and vertical occipital fiber system in more fine detail.

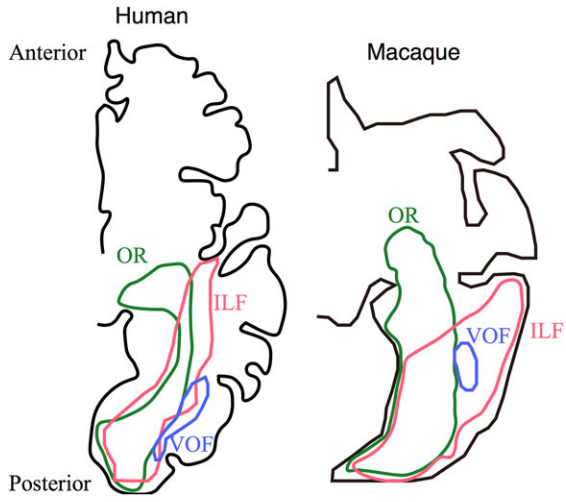

Figure 8. Schematic diagram of estimated human-macaque occipital fiber system. This diagram schematically describes the position of 3 major white-matter pathways in the right hemisphere in humans (left panel) and macaque (right panel); the OR (green), the ILF (red), and the VOF (blue). As compared with macaques, human VOF is moved to the lateral side of the white matter and becomes relatively distinguishable from the ILF.

Combining Postmortem Anatomical Data with in vivo Diffusion MRI

The data in this paper include in vivo diffusion data and postmortem (ex vivo) macaque diffusion data, and we contextualize the diffusion measurements with postmortem tracer studies. Each of these measurement modalities has its own advantages.

The in vivo diffusion data are relatively coarse, but they have great value for studies of development, plasticity, disease, and individual differences in both human and animal studies (Levin et al. 2010; Blumenfeld-Katzir et al. 2011; Li et al. 2011; Yeatman et al. 2012a; Bock et al. 2013; Hofstetter et al. 2013; Sampaio-Baptista et al. 2013; Ogawa et al. 2014; Ajina et al. 2015; Gomez et al. 2015; Warner et al. 2015). The ex vivo diffusion data has advantage in the signal-to-noise ratio, spatial, and angular resolution of the data (Miller et al. 2011; Dell'Acqua et al. 2013; Leuze et al. 2014; Aggarwal et al. 2015; Seehaus et al. 2015).

There are several advantages of ex vivo dMRI compared with other ex vivo anatomical methods, such as tracer methods. First, ex vivo dMRI is useful for a comparison with in vivo dMRI in the same stereotactic space. Second, dMRI provides a large field of view compared with postmortem tracer studies. Third, dMRI and tractography have built up an infrastructure of reproducible computational methods and atlases that can be shared (Calabrese et al. 2015; Hayashi et al. 2015; Reveley et al. 2016). This supports the methods needed to grow a shared database that enables comparisons between individual subjects and population norms (Wandell et al. 2015).

The strengths and weaknesses of invasive anatomical methods are complementary to the dMRI strengths. Postmortem

tracer studies are very well suited for examining hypotheses about the fine spatial detail and directionality of specific connections (Cheng et al. 1997; Ungerleider et al. 2008; Banno et al. 2011; Grimaldi et al. 2016), or the relationship between specific connections and molecular targets (Ichinohe et al. 2010). In contrast, it is very difficult to study the variability between individuals using tracer methods because of the inability to precisely control the placement of injections and uptake of tracers. Anatomical tracer studies typically slice the brain and recover only a subset of the pathways reconstructed from challenging material (Kennedy et al. 2013). Finally, tracer studies have not yet developed a digital technology that enables one to compute atlases and integrate data. The most widely used summaries of anatomical data are simple tables that collect the known collection, and these tables do not capture the pathways themselves (CoCoMac database; Bakker et al. 2012).

One way to proceed is to develop high-resolution models of the visual white-matter tracts using postmortem diffusion data, and to use these models to guide model estimates from lower-resolution in vivo dMRI data. We can then use anatomical tracer methods to analyze specific pathways and cellular molecular questions. To some extent, this approach has been used in much of human tractography. Tractography is often used simply to locate major white-matter tracts that are known to exist, and the properties of these regions are then studied in different groups of subjects or patients (Catani et al. 2002; Wakana et al. 2004; Catani and Thiebaut de Schotten 2008; Yendiki et al. 2011; Yeatman et al. 2012b).

Conclusions

Whereas much of the occipital white matter in human and macaque is similar (OR, forceps major, ILF), we find significant differences. Most significant is the absence in macaque of a tract homologous to human IFOF. The much larger volume (×15) of the human brain seems to have brought forth a need to create a long pathway that speeds the projection of signals from posterior to anterior portions of the brain. Tasks that rely on this communication pathway in human may not have a corresponding substrate in macaque.

A second notable difference is the position of the mVOF and the human VOF with respect to other white-matter tracts. In both species, the VOF connects dorsal and ventral posterior portions of the brain, and are likely to have endpoints near similar maps (V3A and ventral V4). But in human, the VOF is largely segregated from the ILF, while in macaque, the mVOF crosses with the ILF. This difference has implications for interpreting the consequences of white-matter lesions, such as one might observe in stroke patients or other clinical lesions. It is less clear that the position matters for typical signaling and function.

The gross anatomical positions of stimulus-selective cortical regions, such as regions selective for faces, differ between human and macaque (Tsao et al. 2008; Bell et al. 2009; Pinsk et al. 2009; Kornblith et al. 2013; Weiner and Grill-Spector 2015; Lafer-Sousa et al. 2016). The dMRI measurements reveal similarities and differences in the organization of the major occipital white-matter tracts in human and macaque, and the projections of these tracts may explain the different locations of these cortical specializations. As we improve our understanding about the white-matter tracts in both species, we hope to clarify the degree to which the functional circuits we identify in macaque are an accurate model for human vision.

Supplementary Material

Supplementary data is available at *Cerebral Cortex* online.

Author contribution

Designed the study: H.T., F.P., and B.A.W. Performed the experiments: H.T., F.P., G.A.K., S.M.L., J.S., F.Q.Y., D.A.L., W.A.F., and N.K.L. Analyzed the data: H.T., F.P., K.S.W., M.A.B., and B.A.W. Contributed analysis tools: F.P., K.S.W., F.Q.Y., and M.A.B. Wrote the paper: H.T., F.P., K.S.W., and B.A.W.

Funding

This study is funded in part by JSPS Postdoctoral Fellowship for Research Abroad and the Grant-in-Aid for JSPS Research Fellows to H.T., NSF IIS-1636893, and NIH ULTTR001108 to F.P., Human Frontier Science Program Long-Term Fellowship (LT000418/2013-L, to J.S.), a Fondation pour la Recherche Médicale Postdoctoral fellowship (to J.S.), a Women & Science Postdoctoral Fellowship (to J.S.), a Bettencourt-Schueller Foundation Young Researcher Award (to J.S.), the Intramural Research Program of the National Institutes of Health (ZIC MH002899 to F.Q.Y. and D.A.L.), a Pew Scholar Award in the Biomedical Sciences (to W.A.F.), The Esther A. & Joseph Klingenstein Fund (to W.A.F.), a McKnight Scholars Award (to W.A.F.), the New York Stem Cell Foundation (NYSCF-R-NI23, to W.A.F.), the National Eye Institute (R01 EY021594-01A1, to W.A.F.), and NSF BCS-1228397 and a Simons Foundation grant (to B.A.W.). S.M.L. is a Howard Hughes Medical Institute International Student Research fellow. W.A.F. is a New York Stem Cell Foundation-Robertson Investigator. Data were provided in part by the Human Connectome Project, WU-Minn Consortium (Van Essen, D. and Ugurbil, K., 1U54MH091657).

Notes

We thank Ariel Rokem and Jason D. Yeatman for supporting in the collection of human diffusion MRI data, Stelios Smirnakis for supporting in the collection of macaque diffusion MRI data, Kaoru Amano, Atsushi Wada, and Noboru Nushi for providing the computer environment, Cesar F. Caiafa for providing analysis tools, and Lee Michael Perry for technical assistance. *Conflict of Interest*: None declared.

References

Aggarwal M, Nauen DW, Troncoso JC, Mori S. 2015. Probing region-specific microstructure of human cortical areas using high angular and spatial resolution diffusion MRI. Neuroimage. 105:198–207.

Ajina S, Pestilli F, Rokem A, Kennard C, Bridge H, Brown EN. 2015. Human blindsight is mediated by an intact geniculo-extrastriate pathway. eLife Sciences. 4:e08935.

Amano K, Wandell BA, Dumoulin SO. 2009. Visual field maps, population receptive field sizes, and visual field coverage in the human MT+ complex. J Neurophysiol. 102:2704–2718.

Arcaro MJ, McMains SA, Singer BD, Kastner S. 2009. Retinotopic organization of human ventral visual cortex. J Neurosci. 29: 10638–10652.

Bailey P, Von Bonin G, Davis EW, Garol HW, Mcculloch WS. 1944. Further observations on associational pathways in the brain of macaca mulatta. J Neuropathol Exp Neurol. 3:413.

Bakker R, Wachtler T, Diesmann M. 2012. CoCoMac 2.0 and the future of tract-tracing databases. Front Neuroinform. 6:30.

Banno T, Ichinohe N, Rockland KS, Komatsu H. 2011. Reciprocal connectivity of identified color-processing modules in the monkey inferior temporal cortex. Cereb Cortex. 21: 1295–1310.

Bell AH, Hadj-Bouziane F, Frihauf JB, Tootell RBH, Ungerleider LG. 2009. Object representations in the temporal cortex of monkeys and humans as revealed by functional magnetic resonance imaging. J Neurophysiol. 101:688–700.

Berman JI, Lanza MR, Blaskey L, Edgar JC, Roberts TPL. 2013. High angular resolution diffusion imaging probabilistic tractography of the auditory radiation. AJNR Am J Neuroradiol. 34:1573–1578.

Blumenfeld-Katzir T, Pasternak O, Dagan M, Assaf Y. 2011. Diffusion MRI of structural brain plasticity induced by a learning and memory task. PLoS ONE. 6:e20678.

Bock AS, Saenz M, Tungaraza R, Boynton GM, Bridge H, Fine I. 2013. Visual callosal topography in the absence of retinal input. Neuroimage. 81:325–334.

Bonin GV, Garol HW, McCulloch WS. 1942. The functional organization of the occipital lobe. In: Klüver H, editor. Visual mechanisms. Oxford, England: Jacques Cattell. p. 165–192.

Brewer AA, Liu J, Wade AR, Wandell BA. 2005. Visual field maps and stimulus selectivity in human ventral occipital cortex. Nat Neurosci. 8:1102–1109.

Brewer AA, Press WA, Logothetis NK, Wandell BA. 2002. Visual areas in macaque cortex measured using functional magnetic resonance imaging. J Neurosci. 22:10416–10426.

Bullock TH, Bennett MV, Johnston D, Josephson R, Marder E, Fields RD. 2005. Neuroscience. The neuron doctrine, redux. Science. 310:791–793.

Caiafa CF, Pestilli F. 2015. Sparse multiway decomposition for analysis and modeling of diffusion imaging and tractography. ArXiv. 1505:0710.

Caiafa CF, Pestilli F. 2017. Multidimensional encoding of brain connectomes. bioRxiv. 107607.

Calabrese E, Badea A, Coe CL, Lubach GR, Shi Y, Styner MA, Johnson GA. 2015. A diffusion tensor MRI atlas of the postmortem rhesus macaque brain. Neuroimage. 117:408–416.

Catani M, Ffytche DH. 2005. The rises and falls of disconnection syndromes. Brain. 128:2224–2239.

Catani M, Howard RJ, Pajevic S, Jones DK. 2002. Virtual in vivo interactive dissection of white matter fasciculi in the human brain. Neuroimage. 17:77–94.

Catani M, Jones DK, Ffytche DH. 2005. Perisylvian language networks of the human brain. Ann Neurol. 57:8–16.

Catani M, Thiebaut de Schotten M. 2008. A diffusion tensor imaging tractography atlas for virtual in vivo dissections. Cortex. 44:1105–1132.

Catani M, Thiebaut de Schotten M. 2012. Atlas of human brain connections. Oxford: Oxford University Press.

Chamberland M, Scherrer B, Prabhu SP, Madsen J, Fortin D, Whittingstall K, Descoteaux M, Warfield SK. 2017. Active delineation of Meyer's loop using oriented priors through MAGNEtic tractography (MAGNET). Hum Brain Mapp. 38: 509–527.

Cheng K, Saleem KS, Tanaka K. 1997. Organization of corticostriatal and corticoamygdalar projections arising from the anterior inferotemporal area TE of the macaque monkey: a Phaseolus vulgaris Leucoagglutinin Study. J Neurosci. 17: 7902–7295.

Craddock RC, Jbabdi S, Yan CG, Vogelstein JT, Castellanos FX, Di Martino A, Kelly C, Heberlein K, Colcombe S, Milham MP. 2013. Imaging human connectomes at the macroscale. Nat Methods. 10:524–539.

Curran EJ. 1909. A new association fiber tract in the cerebrum with remarks on the fiber tract dissection method of studying the brain. J Comp Neurol Psychol. 19:645–656.

Déjerine J. 1895. Anatomie des centres nerveux. Paris: Rueff et Cie.

Dell'Acqua F, Bodi I, Slater D, Catani M, Modo M. 2013. MR diffusion histology and micro-tractography reveal mesoscale features of the human cerebellum. Cerebellum. 12:923–931.

De Valois RL, Jacobs GH. 1968. Primate color vision. Science. 162:533–540.

De Valois RL, Morgan HC, Polson MC, Mead WR, Hull EM. 1974. Psychophysical studies of monkey vision—I. Macaque luminosity and color vision tests. Vision Res. 14:53–67.

Distler C, Boussaoud D, Desimone R, Ungerleider LG. 1993. Cortical connections of inferior temporal area TEO in macaque monkeys. J Comp Neurol. 334:125–150.

Dougherty RF, Koch VM, Brewer AA, Fischer B, Modersitzki J, Wandell BA. 2003. Visual field representations and locations of visual areas V1/2/3 in human visual cortex. J Vis. 3: 586–598.

Duan Y, Norcia AM, Yeatman JD, Mezer A. 2015. The structural properties of major white matter tracts in strabismic amblyopia. Invest Ophthalmol Vis Sci. 56:5152–5160.

Duffau H, Herbet G, Moritz-Gasser S. 2013. Toward a pluricomponent, multimodal, and dynamic organization of the ventral semantic stream in humans: lessons from stimulation mapping in awake patients. Front Syst Neurosci. 7:44.

Dumoulin SO, Wandell BA. 2008. Population receptive field estimates in human visual cortex. Neuroimage. 39:647–660.

Fields RD. 2008a. White matter matters. Sci Am. 298:42–49.

Fields RD. 2008b. White matter in learning, cognition and psychiatric disorders. Trends Neurosci. 31:361–370.

Fields RD. 2015. A new mechanism of nervous system plasticity: activity-dependent myelination. Nat Rev Neurosci. 16: 756–767.

Forkel SJ, Thiebaut de Schotten M, Kawadler JM, Dell'Acqua F, Danek A, Catani M. 2014. The anatomy of fronto-occipital connections from early blunt dissections to contemporary tractography. Cortex. 56:73–84.

Gellman RS, Carl JR, Miles FA. 1990. Short latency ocular-following responses in man. Vis Neurosci. 5:107–122.

Goda N, Tachibana A, Okazawa G, Komatsu H. 2014. Representation of the material properties of objects in the visual cortex of nonhuman primates. J Neurosci. 34:2660–2673.

Goddard E, Mannion DJ, McDonald JS, Solomon SG, Clifford CW. 2011. Color responsiveness argues against a dorsal component of human V4. J Vis. 11(4):3.

Gomez J, Pestilli F, Witthoft N, Golarai G, Liberman A, Poltoratski S, Yoon J, Grill-Spector K. 2015. Functionally defined white matter reveals segregated pathways in human ventral temporal cortex associated with category-specific processing. Neuron. 85:216–227.

Goodale MA, Milner AD. 1992. Separate visual pathways for perception and action. Trends Neurosci. 15:20–25.

Greenberg AS, Verstynen T, Chiu YC, Yantis S, Schneider W, Behrmann M. 2012. Visuotopic cortical connectivity underlying attention revealed with white-matter tractography. J Neurosci. 32:2773–2782.

Grill-Spector K, Kushnir T, Edelman S, Itzchak Y, Malach R. 1998. Cue-invariant activation in object-related areas of the human occipital lobe. Neuron. 21:191–202.

Grill-Spector K, Kushnir T, Hendler T, Malach R. 2000. The dynamics of object-selective activation correlate with recognition performance in humans. Nat Neurosci. 3:837–843.

Grimaldi P, Saleem KS, Tsao D. 2016. Anatomical connections of the functionally defined "face patches" in the macaque monkey. Neuron. 90:1325–1342.

Hayashi T, Zhang G, Urayama S, Ose T, Watabe H, Onoe K, Tanki N, Murata Y, Higo N, Onoe H 2015. High-resolution diffusion and structural MRI brain atlas of rhesus macaques. Organization for the Human Brain Mapping, Honolulu, HI.

Hofstetter S, Tavor I, Tzur Moryosef S, Assaf Y. 2013. Short-term learning induces white matter plasticity in the fornix. J Neurosci. 33:12844–12850.

Horwitz GD. 2015. What studies of macaque monkeys have told us about human color vision. Neuroscience. 296:110–115.

Ichinohe N, Matsushita A, Ohta K, Rockland KS. 2010. Pathway-specific utilization of synaptic zinc in the macaque ventral visual cortical areas. Cereb Cortex. 20:2818–2831.

Iwai E, Mishkin M. 1969. Further evidence on the locus of the visual area in the temporal lobe of the monkey. Exp Neurol. 25:585–594.

Jbabdi S, Lehman JF, Haber SN, Behrens TE. 2013. Human and monkey ventral prefrontal fibers use the same organizational principles to reach their targets: tracing versus tractography. J Neurosci. 33:3190–3201.

Kay KN, Yeatman JD. 2017. Bottom-up and top-down computations in word- and face-selective cortex. eLife Sciences. 6:e22341.

Kennedy H, Knoblauch K, Toroczkai Z. 2013. Why data coherence and quality is critical for understanding interareal cortical networks. Neuroimage. 80:37–45.

Kim M, Ronen I, Ugurbil K, Kim D-S. 2006. Spatial resolution dependence of DTI tractography in human occipito-callosal region. Neuroimage. 32:1243–1249.

Kolster H, Janssens T, Orban GA, Vanduffel W. 2014. The retinotopic organization of macaque occipitotemporal cortex anterior to V4 and caudoventral to the middle temporal (MT) cluster. J Neurosci. 34:10168–10191.

Konen CS, Kastner S. 2008. Two hierarchically organized neural systems for object information in human visual cortex. Nat Neurosci. 11:224–231.

Kornblith S, Cheng X, Ohayon S, Tsao DY. 2013. A network for scene processing in the macaque temporal lobe. Neuron. 79: 766–781.

Kriegeskorte N, Mur M, Ruff DA, Kiani R, Bodurka J, Esteky H, Tanaka K, Bandettini PA. 2008. Matching categorical object representations in inferior temporal cortex of man and monkey. Neuron. 60:1126–1141.

Lafer-Sousa R, Conway BR, Kanwisher NG. 2016. Color-biased regions of the ventral visual pathway lie between face-and place-selective regions in humans, as in macaques. J Neurosci. 36:1682–1697.

Larsson J, Heeger DJ. 2006. Two retinotopic visual areas in human lateral occipital cortex. J Neurosci. 26:13128–13142.

Lebel C, Benner T, Beaulieu C. 2012. Six is enough? Comparison of diffusion parameters measured using six or more diffusion-encoding gradient directions with deterministic tractography. Magn Reson Med. 68:474–483.

Lee Masson H, Wallraven C, Petit L. 2017. "Can touch this": cross-modal shape categorization performance is associated with microstructural characteristics of white matter association pathways. Hum Brain Mapp. 38:842–854.

Leong JK, Pestilli F, Wu CC, Samanez-Larkin GR, Knutson B. 2016. White-matter tract connecting anterior insula to nucleus accumbens correlates with reduced preference for positively skewed gambles. Neuron. 89:63–69.

Leuze CW, Anwander A, Bazin PL, Dhital B, Stuber C, Reimann K, Geyer S, Turner R. 2014. Layer-specific intracortical connectivity revealed with diffusion MRI. Cereb Cortex. 24:328–339.

Levin N, Dumoulin SO, Winawer J, Dougherty RF, Wandell BA. 2010. Cortical maps and white matter tracts following long period of visual deprivation and retinal image restoration. Neuron. 65:21–31.

Li C, Zhang X, Komery A, Li Y, Novembre FJ, Herndon JG. 2011. Longitudinal diffusion tensor imaging and perfusion MRI investigation in a macaque model of neuro-AIDS: a preliminary study. Neuroimage. 58:286–292.

Li L, Hu X, Preuss TM, Glasser MF, Damen FW, Qiu Y, Rilling J. 2013. Mapping putative hubs in human, chimpanzee and rhesus macaque connectomes via diffusion tractography. Neuroimage. 80:462–474.

Lindbloom-Brown Z, Tait LJ, Horwitz GD. 2014. Spectral sensitivity differences between rhesus monkeys and humans: implications for neurophysiology. J Neurophysiol. 112:3164–3172.

Lyon DC, Connolly JD. 2012. The case for primate V3. Proc Biol Sci. 279:625–633.

Mantini D, Corbetta M, Romani GL, Orban GA, Vanduffel W. 2012. Data-driven analysis of analogous brain networks in monkeys and humans during natural vision. Neuroimage. 63:1107–1118.

Mars RB, Foxley S, Verhagen L, Jbabdi S, Sallet J, Noonan MP, Neubert F-X, Andersson JL, Croxson PL, Dunbar RIM, et al. 2016. The extreme capsule fiber complex in humans and macaque monkeys: a comparative diffusion MRI tractography study. Brain Struct Funct. 221:4059–4071.

Martino J, Brogna C, Robles SG, Vergani F, Duffau H. 2010a. Anatomic dissection of the inferior fronto-occipital fasciculus revisited in the lights of brain stimulation data. Cortex. 46:691–699.

Martino J, Vergani F, Robles SG, Duffau H. 2010b. New insights into the anatomic dissection of the temporal stem with special emphasis on the inferior fronto-occipital fasciculus: implications in surgical approach. Neurosurgery. 66: ons4–ons12.

Martino J, De Witt Hamer PC, Vergani F, Brogna C, de Lucas EM, Vazquez-Barquero A, Garcia-Porrero JA, Duffau H. 2011. Cortex-sparing fiber dissection: an improved method for the study of white matter anatomy in the human brain. J Anat. 219:531–541.

Martino J, Garcia-Porrero JA. 2013. In reply: Wernicke's perpendicular fasciculus and vertical portion of the superior longitudinal fasciculus. Neurosurgery. 73:E382–E383.

Miller KL, Stagg CJ, Douaud G, Jbabdi S, Smith SM, TEJ Behrens, Jenkinson M, Chance SA, Esiri MM, Voets NL, et al. 2011. Diffusion imaging of whole, post-mortem human brains on a clinical MRI scanner. Neuroimage. 57:167–181.

Miura K, Matsuura K, Taki M, Tabata H, Inaba N, Kawano K, Miles FA. 2006. The visual motion detectors underlying ocular following responses in monkeys. Vision Res. 46:869–878.

Mori S, Zhang J. 2006. Principles of diffusion tensor imaging and its applications to basic neuroscience research. Neuron. 51: 527–539.

Newsome WT, Britten KH, Movshon JA. 1989. Neuronal correlates of a perceptual decision. Nature. 341:52–54.

Ogawa S, Takemura H, Horiguchi H, Terao M, Haji T, Pestilli F, Yeatman JD, Tsuneoka H, Wandell BA, Masuda Y. 2014. White matter consequences of retinal receptor and ganglion cell damage. Invest Ophthalmol Vis Sci. 55:6976–6986.

Okazawa G, Goda N, Komatsu H. 2012. Selective responses to specular surfaces in the macaque visual cortex revealed by fMRI. Neuroimage. 63:1321–1333.

Orban GA, Van Essen D, Vanduffel W. 2004. Comparative mapping of higher visual areas in monkeys and humans. Trends Cogn Sci. 8:315–324.

Pajevic S, Pierpaoli C. 1999. Color schemes to represent the orientation of anisotropic tissues from diffusion tensor data: application to white matter fiber tract mapping in the human brain. Magn Reson Med. 42:526–540.

Pestilli F, Yeatman JD, Rokem A, Kay KN, Wandell BA. 2014. Evaluation and statistical inference for human connectomes. Nat Methods. 11:1058–1063.

Petr R, Holden LB, Jirout J. 1949. The efferent intercortical connections of the superficial cortex of the temporal lobe (macaca mulatta)*. J Neuropathol Exp Neurol. 8:100–103.

Pinsk MA, Arcaro M, Weiner KS, Kalkus JF, Inati SJ, Gross CG, Kastner S. 2009. Neural representations of faces and body parts in macaque and human cortex: a comparative FMRI study. J Neurophysiol. 101:2581–2600.

Polosecki P, Moeller S, Schweers N, Romanski LM, Tsao DY, Freiwald WA. 2013. Faces in motion: selectivity of macaque and human face processing areas for dynamic stimuli. J Neurosci. 33:11768–11773.

Press WA, Brewer AA, Dougherty RF, Wade AR, Wandell BA. 2001. Visual areas and spatial summation in human visual cortex. Vision Res. 41:1321–1332.

Rajalingham R, Schmidt K, DiCarlo JJ. 2015. Comparison of object recognition behavior in human and monkey. J Neurosci. 35:12127–12136.

Reveley C, Gruslys A, Ye FQ, Glen D, Samaha J, Russ BE, Saad Z, Seth AK, Leopold DA, Saleem KS. 2016. Three-dimensional digital template atlas of the macaque brain. Cereb Cortex. 1–15. doi: 10.1093/cercor/bhw248.

Reveley C, Seth AK, Pierpaoli C, Silva AC, Yu D, Saunders RC, Leopold DA, Ye FQ. 2015. Superficial white matter fiber systems impede detection of long-range cortical connections in diffusion MR tractography. Proc Natl Acad Sci USA. 112: E2820–E2828.

Rilling JK, Glasser MF, Preuss TM, Ma X, Zhao T, Hu X, Behrens TEJ. 2008. The evolution of the arcuate fasciculus revealed with comparative DTI. Nat Neurosci. 11:426–428.

Roebroeck A, Galuske R, Formisano E, Chiry O, Bratzke H, Ronen I, Kim D-S, Goebel R. 2008. High-resolution diffusion tensor imaging and tractography of the human optic chiasm at 9.4 T. Neuroimage. 39:157–168.

Rokem A, Takemura H, Bock AS, Scherf KS, Behrmann M, Wandell BA, Fine I, Bridge H, Pestilli F. 2017. The visual white matter: the application of diffusion MRI and fiber tractography to vision science. J Vis. 17(2):4.

Russ BE, Leopold DA. 2015. Functional MRI mapping of dynamic visual features during natural viewing in the macaque. Neuroimage. 109:84–94.

Saleem KS, Logothetis NK. 2012. A combined MRI and histology atlas of the rhesus monkey brain in stereotaxic coordinates. San Diego: Academic Press.

Sampaio-Baptista C, Khrapitchev AA, Foxley S, Schlagheck T, Scholz J, Jbabdi S, DeLuca GC, Miller KL, Taylor A, Thomas N, et al. 2013. Motor skill learning induces changes in white matter microstructure and myelination. J Neurosci. 33: 19499–19503.

Sarubbo S, De Benedictis A, Maldonado IL, Basso G, Duffau H. 2013. Frontal terminations for the inferior fronto-occipital fascicle: anatomical dissection, DTI study and functional considerations on a multi-component bundle. Brain Struct Funct. 218:21–37.

Sasaki Y, Rajimehr R, Kim BW, Ekstrom LB, Vanduffel W, Tootell RBH. 2006. The radial bias: a different slant on visual orientation sensitivity in human and nonhuman primates. Neuron. 51:661–670.

Schmahmann JD, Pandya D. 2006. Fiber pathways of the brain. New York: Oxford Univ Press.

Schmahmann JD, Pandya DN, Wang R, Dai G, D'Arceuil HE, de Crespigny AJ, Wedeen VJ. 2007. Association fibre pathways of the brain: parallel observations from diffusion spectrum imaging and autoradiography. Brain. 130:630–653.

Seehaus A, Roebroeck A, Bastiani M, Fonseca L, Bratzke H, Lori N, Vilanova A, Goebel R, Galuske R. 2015. Histological validation of high-resolution DTI in human post mortem tissue. Front Neuroanat. 9:98.

Sherbondy AJ, Dougherty RF, Ben-Shachar M, Napel S, Wandell BA. 2008a. ConTrack: finding the most likely pathways between brain regions using diffusion tractography. J Vis. 8(9):15.

Sherbondy AJ, Dougherty RF, Napel S, Wandell BA. 2008b. Identifying the human optic radiation using diffusion imaging and fiber tractography. J Vis. 8(10):12.

Sigala N, Gabbiani F, Logothetis NK. 2002. Visual categorization and object representation in monkeys and humans. J Cogn Neurosci. 14:187–198.

Silson EH, McKeefry DJ, Rodgers J, Gouws AD, Hymers M, Morland AB. 2013. Specialized and independent processing of orientation and shape in visual field maps LO1 and LO2. Nat Neurosci. 16:267–269.

Smith AT, Greenlee MW, Singh KD, Kraemer FM, Hennig J. 1998. The processing of first- and second-order motion in human visual cortex assessed by functional magnetic resonance imaging (fMRI). J Neurosci. 18:3816–3830.

Sotiropoulos SN, Hernández-Fernández M, Vu AT, Andersson JL, Moeller S, Yacoub E, Lenglet C, Ugurbil K, Behrens TEJ, Jbabdi S. 2016. Fusion in diffusion MRI for improved fibre orientation estimation: an application to the 3 and 7 T data of the Human Connectome Project. Neuroimage. 134:396–409.

Sotiropoulos SN, Jbabdi S, Xu J, Andersson JL, Moeller S, Auerbach EJ, Glasser MF, Hernandez M, Sapiro G, Jenkinson M, et al. 2013. Advances in diffusion MRI acquisition and processing in the Human Connectome Project. Neuroimage. 80: 125–143.

Takemura H, Ashida H, Amano K, Kitaoka A, Murakami I. 2012. Neural correlates of induced motion perception in the human brain. J Neurosci. 32:14344–14354.

Takemura H, Caiafa CF, Wandell BA, Pestilli F. 2016a. Ensemble tractography. PLoS Comput Biol. 12:e1004692.

Takemura H, Rokem A, Winawer J, Yeatman JD, Wandell BA, Pestilli F. 2016b. A major human white-matter pathway between dorsal and ventral visual cortex. Cereb Cortex. 26: 2205–2214.

Thiebaut de Schotten M, Dell'Acqua F, Forkel SJ, Simmons A, Vergani F, Murphy DG, Catani M. 2011. A lateralized brain network for visuospatial attention. Nat Neurosci. 14: 1245–1246.

Thomas C, Ye FQ, Irfanoglu MO, Modi P, Saleem KS, Leopold DA, Pierpaoli C. 2014. Anatomical accuracy of brain connections derived from diffusion MRI tractography is inherently limited. Proc Natl Acad Sci U S A. 111:46.

Tootell RB, Mendola JD, Hadjikhani NK, Ledden PJ, Liu AK, Reppas JB, Sereno MI, Dale AM. 1997. Functional analysis of V3A and related areas in human visual cortex. J Neurosci. 17:7060–7078.

Tootell RB, Tsao D, Vanduffel W. 2003. Neuroimaging weighs in: humans meet macaques in "primate" visual cortex. J Neurosci. 23:3981–3989.

Tournier JD, Calamante F, Connelly A. 2012. MRtrix: diffusion tractography in crossing fiber regions. Int J Imaging Syst Technol. 22:53–66.

Tsao DY, Moeller S, Freiwald WA. 2008. Comparing face patch systems in macaques and humans. Proc Natl Acad Sci USA. 105:19514–19519.

Tsao DY, Vanduffel W, Sasaki Y, Fize D, Knutsen TA, Mandeville JB, Wald LL, Dale AM, Rosen BR, Van Essen DC, et al. 2003. Stereopsis activates V3A and caudal intraparietal areas in macaques and humans. Neuron. 39:555–568.

Ungerleider LG, Desimone R. 1986. Cortical connections of visual area MT in the macaque. J Comp Neurol. 248:190–222.

Ungerleider LG, Galkin TW, Desimone R, Gattass R. 2008. Cortical connections of area V4 in the macaque. Cereb Cortex. 18:477–499.

Ungerleider LG, Haxby JV. 1994. "What" and "where" in the human brain. Curr Opin Neurobiol. 4:157–165.

Ungerleider LG, Mishkin M. 1982. Two cortical visual systems. In: Ingle DJ, Goodale MA, Mansfield RJW, editors. The analysis of visual behavior. Cambridge, MA: MIT Press. p. 549–586.

van den Heuvel MP, Bullmore ET, Sporns O. 2016. Comparative connectomics. Trends Cogn Sci. 20:345–361.

Vanduffel W, Fize D, Mandeville JB, Nelissen K, Van Hecke P, Rosen BR, Tootell RB, Orban GA. 2001. Visual motion processing investigated using contrast agent-enhanced fMRI in awake behaving monkeys. Neuron. 32:565–577.

Vanduffel W, Zhu Q, Orban GA. 2014. Monkey cortex through fMRI glasses. Neuron. 83:533–550.

Van Essen DC, Smith SM, Barch DM, Behrens TE, Yacoub E, Ugurbil K, Consortium W, U-Minn HCP. 2013. The WU-Minn Human Connectome Project: an overview. Neuroimage. 80: 62–79.

Vu AT, Auerbach E, Lenglet C, Moeller S, Sotiropoulos SN, Jbabdi S, Andersson J, Yacoub E, Ugurbil K. 2015. High resolution whole brain diffusion imaging at 7T for the Human Connectome Project. Neuroimage. 122:318–331.

Wade A, Augath M, Logothetis N, Wandell B. 2008. fMRI measurements of color in macaque and human. J Vis. 8(10):6.

Wakana S, Jiang H, Nagae-Poetscher LM, van Zijl PC, Mori S. 2004. Fiber tract-based atlas of human white matter anatomy. Radiology. 230:77–87.

Wandell BA. 2016. Clarifying human white matter. Annu Rev Neurosci. 39:103–128.

Wandell BA, Dumoulin SO, Brewer AA. 2007. Visual field maps in human cortex. Neuron. 56:366–383.

Wandell BA, Rokem A, Perry LM, Schaefer G, Dougherty RF. 2015. Data management to support reproducible research. arXiv. 1502:06900. [q-bioQM].

Wandell BA, Winawer J. 2011. Imaging retinotopic maps in the human brain. Vision Res. 51:718–737.

Wandell BA, Yeatman JD. 2013. Biological development of reading circuits. Curr Opin Neurobiol. 23:261–268.

Wang L, Mruczek REB, Arcaro MJ, Kastner S. 2015. Probabilistic maps of visual topography in human cortex. Cereb Cortex. 25:3911–3931.

Warner CE, Kwan WC, Wright D, Johnston LA, Egan GF, Bourne JA. 2015. Preservation of vision by the pulvinar following early-life primary visual cortex lesions. Curr Biol. 25:424–434.

Webster MJ, Bachevalier J, Ungerleider LG. 1994. Connections of inferior temporal areas TEO and TE with parietal and frontal cortex in macaque monkeys. Cereb Cortex. 4:470–483.

Weiner KS, Grill-Spector K. 2015. The evolution of face processing networks. Trends Cogn Sci. 19:240–241.

Weiner KS, Jonas J, Gomez J, Maillard L, Brissart H, Hossu G, Jacques C, Loftus D, Colnat-Coulbois S, Stigliani A, et al. 2016a. The face-processing network is resilient to focal resection of human visual cortex. J Neurosci. 36:8425–8440.

Weiner KS, Yeatman JD, Wandell BA. 2016b. The posterior arcuate fasciculus and the vertical occipital fasciculus. Cortex. http://dx.doi.org/10.1016/j.cortex.2016.03.012.

Wernicke C 1881. Lehrbuch der Gehirnkrankheiten für Aerzte und Studirende. Kassel Theodor Fischer.

Winawer J, Horiguchi H, Sayres RA, Amano K, Wandell BA. 2010. Mapping hV4 and ventral occipital cortex: the venous eclipse. J Vis. 10(5):1.

Winawer J, Witthoft N. 2015. Human V4 and ventral occipital retinotopic maps. Vis Neurosci. 32:E020.

Witthoft N, Nguyen ML, Golarai G, Larocque KF, Liberman A, Smith ME, Grill-Spector K. 2014. Where is human V4? Predicting the location of hV4 and VO1 from cortical folding. Cereb Cortex. 24:2401–2408.

Wu Y, Sun D, Wang Y, Wang Y, Wang Y. 2016. Tracing short connections of the temporo-parieto-occipital region in the human brain using diffusion spectrum imaging and fiber dissection. Brain Res. 1646:152–159.

Yeatman JD, Dougherty RF, Ben-Shachar M, Wandell BA. 2012a. Development of white matter and reading skills. Proc Natl Acad Sci U S A. 109:E3045–E3053.

Yeatman JD, Dougherty RF, Myall NJ, Wandell BA, Feldman HM. 2012b. Tract profiles of white matter properties: automating fiber-tract quantification. PLoS ONE. 7:e49790.

Yeatman JD, Rauschecker AM, Wandell BA. 2013. Anatomy of the visual word form area: adjacent cortical circuits and long-range white matter connections. Brain Lang. 125:146–155.

Yeatman JD, Weiner KS, Pestilli F, Rokem A, Mezer A, Wandell BA. 2014. The vertical occipital fasciculus: a century of controversy resolved by in vivo measurements. Proc Natl Acad Sci USA. 111:E5214–E5223.

Yendiki A, Panneck P, Srinivasan P, Stevens A, Zöllei L, Augustinack J, Wang R, Salat D, Ehrlich S, Behrens T, et al. 2011. Automated probabilistic reconstruction of white-matter pathways in health and disease using an atlas of the underlying anatomy. Front Neuroinform. 5:23.

Zarco W, Merchant H, Prado L, Mendez JC. 2009. Subsecond timing in primates: comparison of interval production between human subjects and rhesus monkeys. J Neurophysiol. 102: 3191–3202.